Enhanced Water Vapor Transport to the Stratosphere by Pollutants in Asia

Hui Su[1*], Jonathan H. Jiang[1], Xiaohong Liu[2], Joyce E. Penner[3], William G. Read[1], Steven Massie[4], Mark R. Schoeberl[5], Peter Colarco[6], Nathaniel J. Livesey[1], Michelle L. Santee[1]

[1]Jet Propulsion Laboratory, California Institute of Technology, Pasadena, CA 91109

[2]Pacific Northwest National Laboratory, Richland, WA

[3]Department of Atmospheric, Oceanic, and Space Sciences, University of Michigan, Ann Arbor, MI

[4]National Center for Atmospheric Research, Boulder, CO

[5]NASA Goddard Space Flight Center (Retired), Greenbelt, MD

[6]NASA Goddard Space Flight Center, Greenbelt, MD

[*]Corresponding author: Hui Su, Jet Propulsion Laboratory, California Institute of Technology, Pasadena, CA, 91109

Email: Hui.Su@jpl.nasa.gov

Abstract. It has been hypothesized that increased aerosols may change cirrus cloud particle size and lifetime, causing higher water vapor abundance in air that enters the stratosphere. Here, we analyze new satellite observations in two regions where Asian pollution prevails: the South and East Asia during boreal summer and the maritime continent during boreal winter. We find that polluted ice clouds have smaller ice effective radius, and higher temperature and specific humidity near the tropopause than clean clouds. Such water vapor enhancement cannot be explained simply by meteorological factors, suggesting aerosol effects on clouds may be responsible. Simulations from a coupled aerosol-climate model confirm that increasing aerosol ice nuclei can produce warmer tropopause temperature and greater water vapor transport into the stratosphere. Thus, the increasing aerosol emissions over Asia may have significant impacts on stratospheric water vapor, and hence ozone chemistry and the global radiation budget.

1. Introduction

Water vapor is a strong greenhouse gas that acts to amplify surface warming caused by anthropogenic greenhouse gases (e.g., CO_2). In the stratosphere, water vapor also plays a major role in ozone chemistry and serves as a reliable dynamical tracer because of its long lifetime. The mechanisms that control the amount of stratospheric water vapor have not been fully understood. Current theory is that the entry value of water vapor mixing ratio into the stratosphere ($[H_2O]_e$) is largely determined by the cold-point tropopause temperature (CPT), through which air is freeze dried during slow ascent from the troposphere to the stratosphere (Holton and Gettelman 2001; Fueglistaler et al. 2005; Randel et al. 2001). Several other processes may modify $[H_2O]_e$. For example, overshooting convection detrains cold and dry air, which dehydrates the stratosphere, while evaporation of detrained small ice crystals may re-hydrate the tropical tropopause layer (TTL) (Sherwood and Dessler 2001; Dessler 2002; Jensen et al. 2007). The radiative heating from

subvisible cirrus clouds near the tropopause can increase $[H_2O]_e$ by increasing tropopause temperature (Rosenfield et al. 1998). A linkage between aerosols and $[H_2O]_e$ was first proposed by Sherwood (2002a). He postulated that aerosols from biomass burning may reduce ice cloud effective radius (R_e) near the top of cumulus towers, leading to a decrease in the settling velocity of ice crystals and an increase in ice sublimation, and thus giving rise to increased $[H_2O]_e$. A modeling study by Notholt et al. (2005) showed that increasing anthropogenic SO_2 emissions in Asia may increase the formation of sulfuric acid aerosols and thus small ice crystals in the TTL, which are lifted into the stratosphere and increase stratospheric humidity when they evaporate. More recently, Liu et al. (2007; 2009) showed that increasing anthropogenic sulfate and soot concentrations in a global aerosol-climate model lead to increased ice clouds and water vapor in the upper troposphere (UT) and lower stratosphere (LS). These studies suggest that aerosol effects on clouds may increase $[H_2O]_e$. In addition, Lau et al. (2006) indicated that direct radiative heating of absorbing aerosols such as dust and black carbon may cause UT moistening over the Tibetan Plateau during the Asian monsoon season. However, observational evidence of aerosol influence on stratospheric water vapor has been lacking.

In this study, we use Aura Microwave Limb Sounder (MLS) water vapor (H_2O), temperature, ice water content (IWC) and carbon monoxide (CO) measurements (V2.2) in the UTLS, and Aqua Moderate-resolution Imaging Spectroradiometer (MODIS) aerosol optical thickness (AOT, MYD04-L2) and R_e (MOD08-D3) data to examine aerosol effects on $[H_2O]_e$. The MLS data have a horizontal resolution of ~300 km along track and ~7 km cross track. The vertical resolutions for H_2O, IWC and CO are about 3 km, 4 km and 5 km, respectively. V2.2 CO at 215 hPa has a factor of 2 high bias but the morphology is validated to be reasonable (Livesey et al. 2008). We average the MODIS data into 3°×1° boxes centered on the MLS measurement locations to obtain

collocated MODIS and MLS measurements. From these observations, we aim to identify several key components of the aerosol and $[H_2O]_e$ linkage, specially, the changes in R_e, temperature and H_2O in the UTLS when aerosol concentration changes. The influence of meteorological conditions on H_2O is examined using Aqua Atmospheric Infrared Sounder (AIRS) measurements and reanalysis data from the National Centers for Environmental Prediction (NCEP). Simulations from a coupled aerosol-climate model are also analyzed to confirm the aerosol effects on $[H_2O]_e$.

2. Analysis of satellite data

We choose two analysis regions, both of which are important pathways for water vapor transport to the stratosphere and experience heavy pollution from Asian countries with rapidly growing economies. One area is South and East Asia (SEA, 60º-130ºE, 10º-40ºN) in June-July-August (JJA), and the other is the maritime continent (MTC, 80ºE-160ºE, 15ºS-15ºN) in December-January-February (DJF).

Figure 1 shows maps of 2005-2008 JJA and DJF average MODIS AOT, MLS CO and IWC at 215 hPa, and MLS water vapor and IWC at 147 and 100 hPa, encompassing the two analysis regions (dashed boxes). The 147 and 100 hPa pressure levels approximately correspond to the bottom of the TTL and the height of the CPT, respectively. During boreal summer, the spatial distribution of 215 hPa CO resembles that of AOT, although enhanced CO is more widespread than high AOT as CO, unlike aerosols, is not subject to wet removal by clouds and precipitation. The SEA region has the highest AOT and CO, coincident with high H_2O and IWC at 147 and 100 hPa. The anticyclone over the Tibetan Plateau traps high CO and H_2O, providing a significant source of trace gases to the stratosphere (Li et al. 2005; Fu et al. 2006; Park et al. 2009). During boreal winter, the MTC region has the coldest CPT and is extremely important in determining $[H_2O]_e$ (the so-called “stratospheric fountain”, Newell and Gould-Stewart 1981). It is also a region

into which Asian pollution is preferentially transported (Stohl et al. 2002). Figure 1e and 1f show that the MLS CO at 215 hPa is quite high over the entire MTC region, while high AOT is concentrated over land (islands) and is relatively low over ocean. The high CO may include pollution advected from South and East Asia at lower levels that is uplifted to the UT by deep convection (indicated by the IWC contours at 215 hPa, also see Figure 2 in Stohl et al. 2002). Water vapor is relatively high over the MTC at 147 hPa because of strong convection, but reaches a minimum at 100 hPa associated with the CPT. Based on the Goddard Earth Observing System Model (Version 5) analyses, the average thermal tropopause height (Figure 1b and 1f) over DJF MTC is around 90-100 hPa, higher than that in JJA SEA.

Following Jiang et al. (2008), we use MLS CO at 215 hPa as a proxy for aerosols to classify ice clouds as "polluted" or "clean". The in-cloud CO bears a close correlation to aerosol loading in many convective regions (Jiang et al. 2009). As in-cloud aerosols are difficult to measure, using CO gives us about 3-4 times the number of samples of collocated pollution, clouds and H_2O than obtained by simply using AOT in adjacent cloud-free regions, ensuring a higher signal to noise ratio and greater statistical significance. Compared to the CO at 147 and 100 hPa, the 215 hPa CO has the strongest correlation with surface emission coincident with convection (Jiang et al. 2007). For this study, we define polluted ice clouds to be the instantaneous measurements that have detectable MLS IWC (the IWC detection thresholds are 0.6 mg/m^3 at 215 hPa, 0.1 mg/m^3 at 147 hPa and 0.02 mg/m^3 at 100 hPa, see Wu et al. 2008) throughout 215 to 100 hPa and MLS CO at 215 hPa greater than 240 ppbv in JJA and 200 ppbv in DJF. By definition, these clouds are mostly deep convective clouds and associated anvils. Clean ice clouds are those meeting the same IWC criterion but with 215 hPa CO less than 120 ppbv in JJA and 100 ppbv in DJF. The average fraction of polluted clouds out of the total valid measurement ensemble is about 3.2% in JJA SEA

(685 profiles) and 1.8% in DJF MTC (449 profiles), and the fraction of clean clouds is close to 1% in both cases (157 profiles in JJA SEA and 236 profiles in DJF MTC). Our definitions of polluted and clean clouds represent the two extreme ends of the cloud spectrum, so that a distinct signal of aerosol effects can be extracted. Clouds that are not "deep" or have intermediate CO values are not considered.

As the UT CO loading reflects the combined effect of convection and surface emissions (Jiang et al. 2007), we compare the polluted and clean cloud properties binned by MLS 215 hPa IWC, which correlates well with outgoing longwave radiation and serves as a measure of convective strength (Jiang et al. 2007; Su et al. 2006). Horizontal advection may complicate the dependence of CO on convection and emission strength. However, for deep clouds with the same IWC, the UT CO difference can mostly be attributed to differences in surface emission (related to AOT) rather than differences in convective strength. Using the NCEP 500 hPa vertical velocity (ω_{500}) or 200 hPa divergence as alternative indices for convective strength produces similar results to those obtained from binning by the 215 hPa IWC (not shown).

Figure 2 shows that polluted clouds are associated with higher AOT than clean clouds for most values of IWC in both regions, except at large IWCs where aerosols are removed by precipitation. The aerosol concentrations are generally higher in SEA than in MTC. The averaged difference in AOT for all IWCs between polluted and clean clouds is about 0.21 (~45%) in SEA and 0.04 (~16%) in MTC. For a given IWC, polluted clouds have smaller R_e than clean clouds, as noted previously (Jiang et al. 2008; 2009). The average R_e difference is about 1-2 μm (5-10%). In JJA SEA, polluted clouds have higher H_2O and temperature than clean clouds at both 147 and 100 hPa; the differences extend up to 83 hPa. In DJF MTC, the increased H_2O and temperature in polluted clouds are evident at 121, 100 and 83 hPa but insignificant at 147 hPa, probably because of the

higher tropopause in this region than in JJA SEA. In both cases, the H_2O difference at 100 hPa is approximately 0.2-0.5 ppmv, and the temperature difference is about 2 K. These differences are comparable to the magnitudes of the interannual anomalies for 100 hPa H_2O and temperature driven by large-scale dynamics (Fueglistaler and Haynes 2005). At 100 hPa, polluted clouds have lower relative humidity with respect to ice (RHi) than clean clouds, as the change in temperature dominates over the change in H_2O.

To test whether the 100 hPa H_2O difference in the polluted and clean clouds may simply arise from different meteorological conditions, we group these clouds by their meteorological conditions rather by their pollution loadings. Figure 3 shows that there is no significant difference in 100 hPa H_2O between the two groups separated by boundary layer (850 hPa) humidity or convective available potential energy (CAPE) based on AIRS data, nor by 850 hPa convergence or ω_{500} from NCEP reanalysis. Only when these clouds are grouped by their pollution loadings, as shown in Figure 2, is a clear separation in 100 hPa H_2O attained. Similar results are found for 83 and 121 hPa H_2O, and for all deep clouds with intermediate CO values.

3. Coupled aerosol-cloud model simulations

We further analyze two aerosol-climate model simulations for the JJA SEA and DJF MTC regions. The simulations are conducted using the National Center for Atmospheric Research (NCAR) Community Atmospheric Model Version 3 (CAM3) coupled with the Lawrence Livermore National Laboratory (LLNL)/University of Michigan IMPACT aerosol model (see Liu et al. 2009 for details). The two model runs employ present-day (PD) and pre-industrial (PI) aerosol and precursor gas emissions, respectively, with all other parameters (e.g., sea surface temperature, greenhouse gas concentrations, solar constant, chemical oxidant concentrations, etc.) prescribed at the same present-day conditions. Both homogeneous ice nucleation on sulfate and

heterogeneous nucleation on ice nuclei (as represented by soot), and the competition between these two ice nucleation mechanisms, are considered in the model (Liu and Penner 2005; Liu et al. 2007). Ice number density changes due to ice nucleation on anthropogenic aersosols alter R_e, and thus the microphysical and optical properties of ice clouds. Inclusion of the aerosol effects in the CAM3 has shown improvements in the model simulated cirrus properties (Liu et al. 2007). Comparing the PD and PI runs, we find that the model produces smaller ice cloud particle sizes, and larger 100 hPa temperature and H_2O when aerosol concentration increases, qualitatively similar to the observations for each region (Figure 4). The physically based simulations represent one scenario by which aerosols alter ice cloud properties and hence $[H_2O]_e$. We note that the model does not consider heterogeneous ice nucleation on ammonium sulfate, or interaction of aerosols with sub-grid scale cumulus towers, which may have additional aerosol impacts on ice clouds and $[H_2O]_e$ (Abbatt et al. 2006; Jensen et al. 2010; Jensen and Ackerman 2006).

4. Discussion and Conclusion

Combining observations and aerosol-climate model simulations, we have presented evidence of increased water vapor transport to the stratosphere by pollutants in Asia. The aerosol-induced $[H_2O]_e$ change in heavily polluted cloudy regions, comparable in magnitude to the interannaul variations of $[H_2O]_e$, is associated with temperature changes near the tropopause. The exact pathways for the aerosol-cloud-$[H_2O]_e$ interactions are not known. Here, we propose a plausible mechanism as follows (Figure 5). Increasing aerosols increase cloud condensation nuclei numer density and reduce R_e. As Sherwood (2002b) argued, even if the aerosols are concentrated in the lower troposphere, they may still exert changes in ice cloud particle size by changing the effective radius of liquid cloud droplets, which can be lofted above the freezing levels to form ice crystals. Smaller ice particles fall more slowly and have longer residence times, causing greater radiative

heating and higher temperature in the TTL. The increased TTL radiative heating may accelerate vertical ascent from the troposphere to the stratosphere (Corti et al. 2006). Meanwhile, smaller ice particles evaporate more rapidly, increasing humidity. Hence, three processes need further corroboration: increased TTL radiative heating, accelerated vertical ascent, and enhanced ice evaporation in polluted clouds. Current observations cannot fully determine the relative role of each process. Improvements in the treatment of aerosol-cloud interactions in models are also needed. We note that stratospheric water vapor is influenced not just by aerosols. Natural variability associated with large-scale dynamics strongly controls stratospheric water vapor changes (e.g. Fueglistaler and Haynes 2005; Solomon et al. 2010). How changes in Asian pollution contribute to the global stratospheric water vapor variations warrants further study.

Acknowledgements

We thank the funding support from the NASA ACMAP, AST and IDS programs. XL and JEP acknowledge the support from DOE ARM Program. Discussions with Daniel Rosenfeld are greatly appreciated. This work was performed at Jet Propulsion Laboratory, California Institute of Technology, under contract with NASA.

References

Abbatt, J. P. D., Benz, S., Cziczo, D. J., Kanji, Z., Lohmann, U., and O. Mohler, O.: Solid ammonium sulfate aerosols as ice nuclei: A pathway for cirrus formation, *Science*, 313, 1770–1773 (2006).

Corti, T., B. P. Luo, Q. Fu, H. Vomel, and T. Peter, The impact of cirrus clouds on tropical troposphere to stratosphere transport, *Atmos. Chem. Phys*., 6, 2539–2547 (2006).

Dessler, A. E., The effect of deep, tropical convection on the tropical tropopause layer, *J. Geophys. Res.*, 107(D3), 4033, doi:10.1029/2001JD000511 (2002).

Fu, R., et al., Short circuit of water vapor and polluted air to the global stratosphere by convective transport over the Tibetan Plateau, *Proc. Nat. Acad. Sci.*, **103**, 5664-5669 (2006).

Fueglistaler, S., and P. H. Haynes, Control of interannual and longer-term variability of stratospheric water vapor, *J. Geophys. Res*., 110, D24108, doi:10.1029/2005JD006019 (2005).

Fueglistaler, S., Bonazzola, M., Haynes, P. H., and Peter, T.: Stratospheric water vapor predicted from the Lagrangian temperature history of air entering the stratosphere in the tropics, *J. Geophys. Res.*, **110**, D08107, doi:10.1029/2004JD005516 (2005).

Holton, J. R., and A. Gettelman, Horizontal transport and the dehydration of the stratosphere, *Geophys. Res. Lett*., **28**, 2799-2802 (2001).

Jensen, E. J., A. S. Ackerman, and J. A. Smith, Can overshooting convection dehydrate the tropical tropopause layer? *J. Geophys. Res.*, **112**, D11209, doi:10.1029/2006JD007943 (2007).

Jensen, E. J., and A. S. Ackerman (2006), Homogeneous aerosol freezing in the tops of high-altitude tropical cumulonimbus clouds, *Geophys. Res. Lett*., 33, L08802, doi:10.1029/2005GL024928 (2006).

Jensen E. et al., Ice nucleation and cloud microphysical properties in tropical tropopause layer cirrus, *Atmos. Chem. Phys.* 10, 1369-1384 (2010).

Jiang, J.H., H. Su, M. Schoeberl, S.T. Massie, P. Colarco, S. Platnick, and N. Livesey, Clean and polluted clouds: relationships among pollution, ice cloud and precipitation in South America, *Geophys. Res. Lett.* **35**, L14804, doi:10.1029/2008GL034631 (2008).

Jiang, J.H., H. Su, S.T. Massie, P. Colarco, M. Schoeberl, and S. Platnick, Aerosol-CO Relationship and Aerosol Effect on Ice Cloud Particle Size: Analyses from Aura MLS and Aqua MODIS Observations, *J. Geophys. Res.*, **114**, D20207, doi:10.1029/2009JD012421, (2009).

Jiang, J.H., N.J. Livesey, H. Su, L. Neary, J.C. McConnell, and N.A. Richards, Connecting surface emissions, convective uplifting, and long-range transport of carbon monoxide in the upper troposphere: New observations from the Aura Microwave Limb Sounder, *Geophys. Res. Lett.* **34**, L18812, doi:10.1029/2007GL030638 (2007).

Lau, K. M. and K. M. Kim, Observational relationships between aerosol and Asian monsoon rainfall, and circulation, *Geophys. Res. Lett.*, **33**, L21810, doi:10.1029/2006GL027546 (2006).

Li, Q.B., et al., Convective outflow of South Asian pollution: A global CTM simulation compared with EOS MLS observations, *Geophys. Res. Lett*., **32**, L14826, doi:10.1029/2005GL022762 (2005).

Liu, X., J. E. Penner, and M. Wang, Influence of anthropogenic sulfate and black carbon on upper tropospheric clouds in the NCAR CAM3 model coupled to the IMPACT global aerosol model, *J. Geophys. Res.*, **114**, D03204, doi:10.1029/2008JD010492 (2009).

Liu, X., J. E. Penner, S. J. Ghan, and M. Wang, Inclusion of Ice Microphysics in the NCAR Community Atmospheric Model Version 3 (CAM3), *J. Climate*, 20, 4526-4547 (2007).

Liu, X., and J. E. Penner, Ice nucleation parameterization for global models. *Meteorologische Zeitschrift*, Vol. 14, No.4, 499-514 (2005).

Newell, R. E., and S. Gould-Stewart, A stratospheric fountain? *J. Atmos. Sci.,* **51**, 2789- 2796 (1981).

Livesey, N.J., et al., Validation of Aura Microwave Limb Sounder O3 and CO observations in the upper troposphere and lower stratosphere, *J. Geophys. Res.* **113**, D15S02, doi:10.1029/2007JD008805 (2008).

Notholt J., et al., Influence of tropospheric SO_2 emissions on particle formation and the stratospheric humidity, *Geophys. Res. Lett.,* **32**, L07810, doi:10.1029/2004GL022159 (2005).

Park, M., W.J. Randel, L.K. Emmons, and N.J. Livesey, Transport pathways of carbon monoxide in the Asian summer monsoon diagnosed from Model of Ozone and Related Tracers (MOZART), *J. Geophys. Res*. **114**, D08303, doi:10.1029/2008JD010621 (2009).

Randel, W. J., Wu, F., Vomel, H., Nedoluha, G. E., and Forster, P.: Decreases in Stratospheric Water Vapor after 2001: Links to Changes in the Tropical Tropopause and the Brewer-Dobson Circulation, *J. Geophys. Res*., **111**, D12312, doi:10.1029/2005JD006744, 2006.

Rosenfield, J., D. Considine, M. Schoeberl, and E. Browell, The Impact of Subvisible Cirrus Clouds Near the Tropical Tropopause on Stratospheric Water Vapor, *Geophys. Res. Lett.*, **25**, 1883-1886 (1998).

Sherwood, S. C. and A. E. Dessler: A model for transport across the tropical tropopause, *J. Atmos. Sci*., **58**, 765–779 (2001).

Sherwood, S., A microphysical connection among biomass burning, cumulus clouds, and stratospheric moisture, *Science*, **295**, 1272-1275 (2002a).

Sherwood, S.C., Aerosols and ice particle size in tropical cumulonimbus. *J. Clim*, **15**, 1051-1063 (2002b).

Solomon, S., K. Rosenlof, R. Portmann, J. Daniel, S. Davis, T. Sanford, and G. Plattner, Contributions of Stratospheric Water Vapor to Decadal Changes in the Rate of Global Warming, *Science*, **303,** (2010).

Stohl, A., S. Eckhardt, C. Forster, P. James, N. Spichtinger, On the pathways and timescales of intercontinental air pollution transport. *J. Geophys. Res*. **107**, 4684, doi:10.1029/2001JD001396 (2002).

Su, H., W.G. Read, J.H. Jiang, J.W. Waters, D.L. Wu, and E.J. Fetzer, Enhanced positive water vapor feedback associated with tropical deep convection, New evidence from Aura MLS, *Geophys. Res. Lett.*, **33**, L05709, doi:10.1029/2005GL025505 (2006).

Wu, D.L., J.H. Jiang, W.G. Read, R.T. Austin, C.P. Davis, A. Lambert, G.L. Stephens, D.G. Vane, and J.W. Waters, Validation of the Aura MLS Cloud Ice Water Content (IWC) Measurements, *J. Geophys. Res.* **113**, doi:10.1029/2007JD008931 (2008).

Figure Captions

Figure 1. Maps of AOT, UT CO, H_2O and IWC averaged for 2005 to 2008, with the top row for JJA and the bottom row for DJF. (a) and (e) MODIS AOT; (b) and (f) MLS 215 hPa CO (shaded) and IWC (black contours at 2 mg/m^3 interval), with white contours indicating the GEOS-5 lapse-rate tropopause pressure; (c) and (g) MLS 147 hPa H_2O (shaded) and IWC (black contours at 1 mg/m^3 interval); (d) and (h) MLS 100 hPa H_2O (shaded) and IWC (black contours at 0.2 mg/m^3 interval), with white contours indicating MLS temperature at 100 hPa. The analysis region in each season is marked by the dashed box**.**

Figure 2. AOT, ice cloud particle size, TTL H_2O and temperature for polluted and clean clouds, binned on the 215 hPa MLS IWC, with the top row for JJA South and East Asia (SEA) and the bottom row for DJF maritime continent (MTC). (a) and (e) MODIS AOT; (b) and (f) MODIS ice cloud effective radius (R_e); (c) and (g) MLS temperature; (d) and (h) MLS H_2O. The error bars denote the standard errors ($\sigma/\sqrt{N}$) of the bin averages.

Figure 3. 100 hPa H_2O for polluted and clean clouds grouped by their meteorological conditions. (a) by AIRS 850 hPa water vapor mixing ratio; (b) by NCEP divergence at 850 hPa; (c) by NCEP ω_{500}; and (d) by CAPE calculated from AIRS temperature and water vapor soundings. The choice of threshold values for each grouping ensures approximately the same number of samples for each group. All properties are binned on the 215 hPa MLS IWC, with the top row for JJA SEA and the bottom row for DJF MTC. The error bars denote the standard errors ($\sigma/\sqrt{N}$) of the bin averages.

Figure 4. AOT, ice cloud particle size, 100 hPa temperature and H_2O for the present day (PD) and pre-industrial (PI) runs, binned on the simulated 215 hPa IWC, with the top row for JJA SEA and the bottom row for DJF MTC. Only "deep" clouds with non-zero IWC throughout 215 and 100 hPa are considered. (a) and (e) AOT; (b) and (f) Averaged R_e for ice clouds within 215 and 100

hPa; (c) and (g) 100 hPa temperature; (d) and (h) 100 hPa H_2O. The error bars denote the standard errors ($\sigma/\sqrt{N}$) of the bin averages.

Figure 5. A schematic illustration of the modification of water vapor transport to the stratosphere by aerosol effects on clouds. Higher aerosol concentrations cause smaller cloud particles which fall more slowly. Compared to clean clouds, polluted clouds have greater radiative heating in the TTL, which causes higher temperature and faster ascent into the stratosphere. Smaller ice particles also evaporate more rapidly. Combining these effects together, polluted clouds induce enhanced water vapor transport into the stratosphere compared to clean clouds.

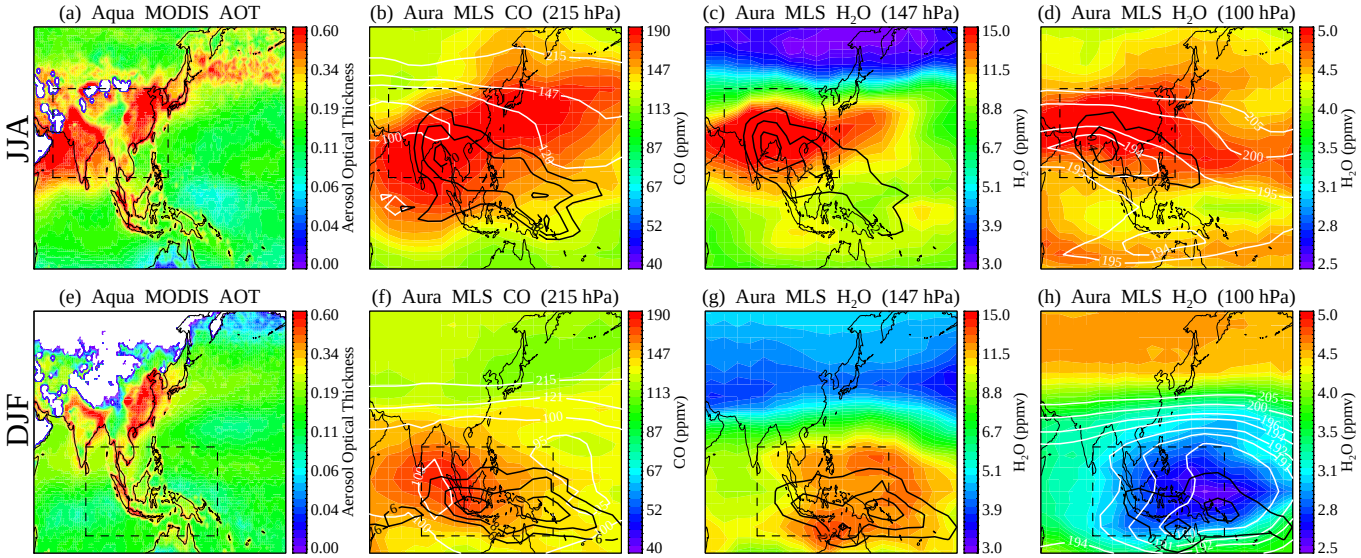
(a) Aqua MODIS AOT
(b) Aura MLS CO (215 hPa)
(c) Aura MLS H2O (147 hPa)
(d) Aura MLS H2O (100 hPa)
(e) Aqua MODIS AOT
(f) Aura MLS CO (215 hPa)
(g) Aura MLS H2O (147 hPa)
(h) Aura MLS H2O (100 hPa)
JJA
DJF
Aerosol Optical Thickness
0.60
0.34
0.19
0.11
0.06
0.04
0.00
CO (ppmv)
190
147
113
87
67
52
40
H2O (ppmv)
15.0
11.5
8.8
6.7
5.1
3.9
3.0
5.0
4.5
4.0
3.5
3.1
2.8
2.5

Figure 1

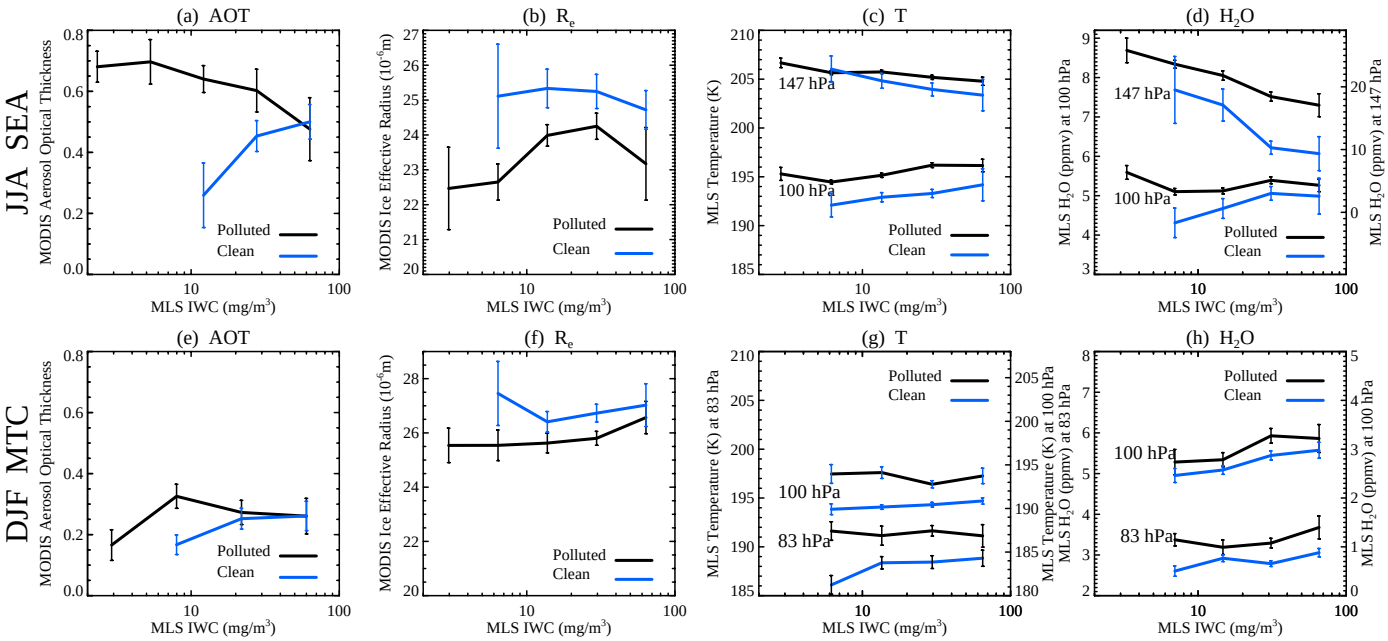
JJA SEA
DJF MTC
(a) AOT
(b) R_e
(c) T
(d) H_2O
(e) AOT
(f) R_e
(g) T
(h) H_2O
MODIS Aerosol Optical Thickness
MODIS Ice Effective Radius (10^{-6}m)
MLS Temperature (K)
MLS H_2O (ppmv) at 100 hPa
MLS H_2O (ppmv) at 147 hPa
MLS Temperature (K) at 83 hPa
MLS Temperature (K) at 100 hPa
MLS H_2O (ppmv) at 83 hPa
MLS H_2O (ppmv) at 100 hPa
MLS IWC (mg/m^3)
Polluted
Clean
147 hPa
100 hPa
83 hPa

Figure 2

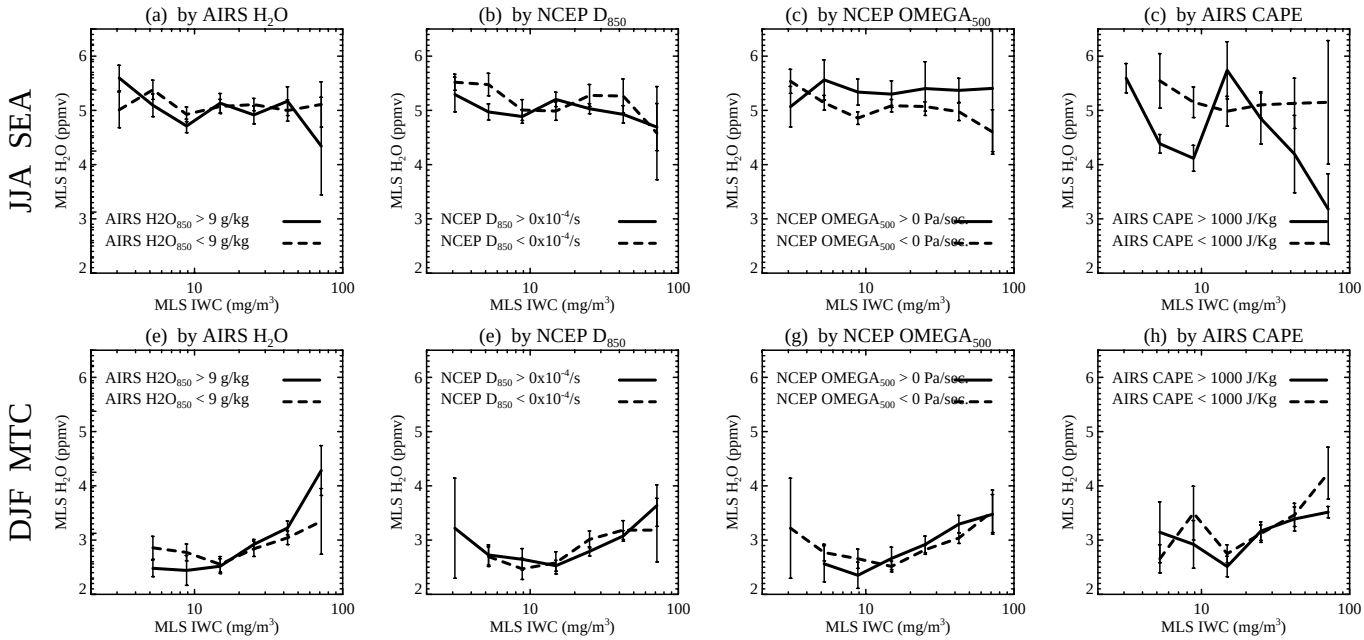
JJA SEA
DJF MTC
(a) by AIRS H2O
(b) by NCEP D850
(c) by NCEP OMEGA500
(c) by AIRS CAPE
(e) by AIRS H2O
(e) by NCEP D850
(g) by NCEP OMEGA500
(h) by AIRS CAPE
MLS H2O (ppmv)
MLS IWC (mg/m3)
AIRS H2O850 > 9 g/kg
AIRS H2O850 < 9 g/kg
NCEP D850 > 0x10-4/s
NCEP D850 < 0x10-4/s
NCEP OMEGA500 > 0 Pa/sec.
NCEP OMEGA500 < 0 Pa/sec.
AIRS CAPE > 1000 J/Kg
AIRS CAPE < 1000 J/Kg

Figure 3

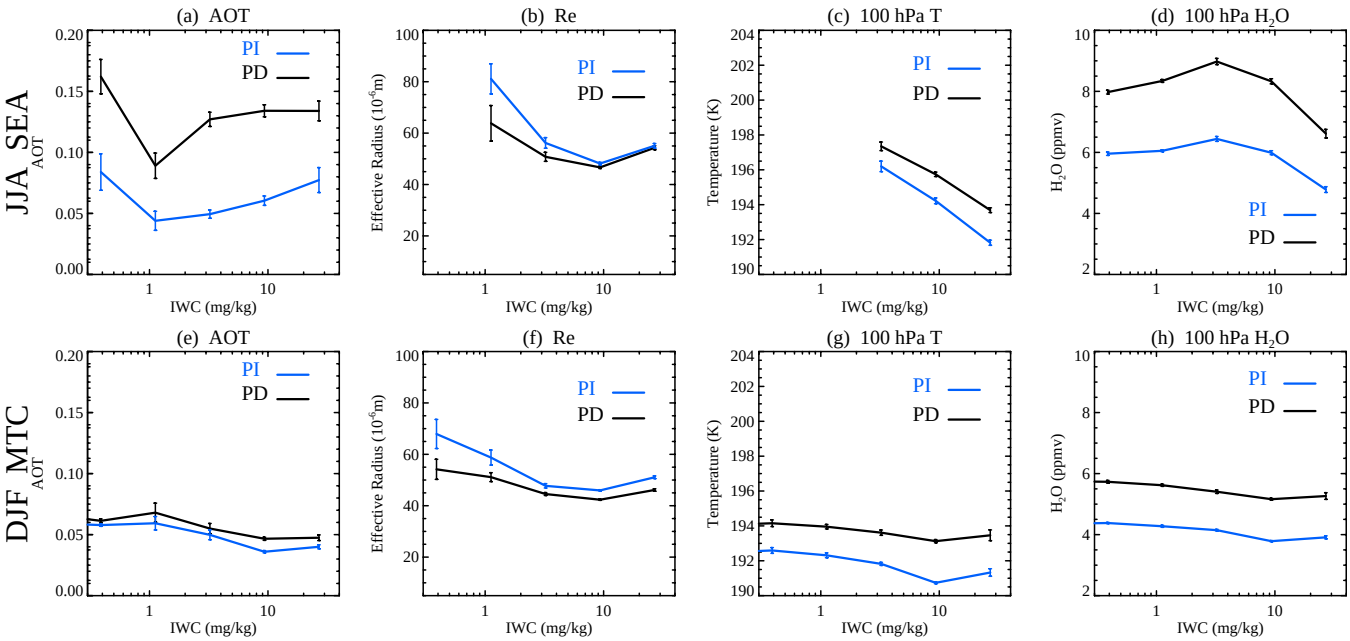
(a) AOT
(b) Re
(c) 100 hPa T
(d) 100 hPa H2O
(e) AOT
(f) Re
(g) 100 hPa T
(h) 100 hPa H2O
JJA_SEA
DJF_MTC
AOT
PI
PD
IWC (mg/kg)
Effective Radius (10^-6 m)
Temperature (K)
H2O (ppmv)

Figure 4

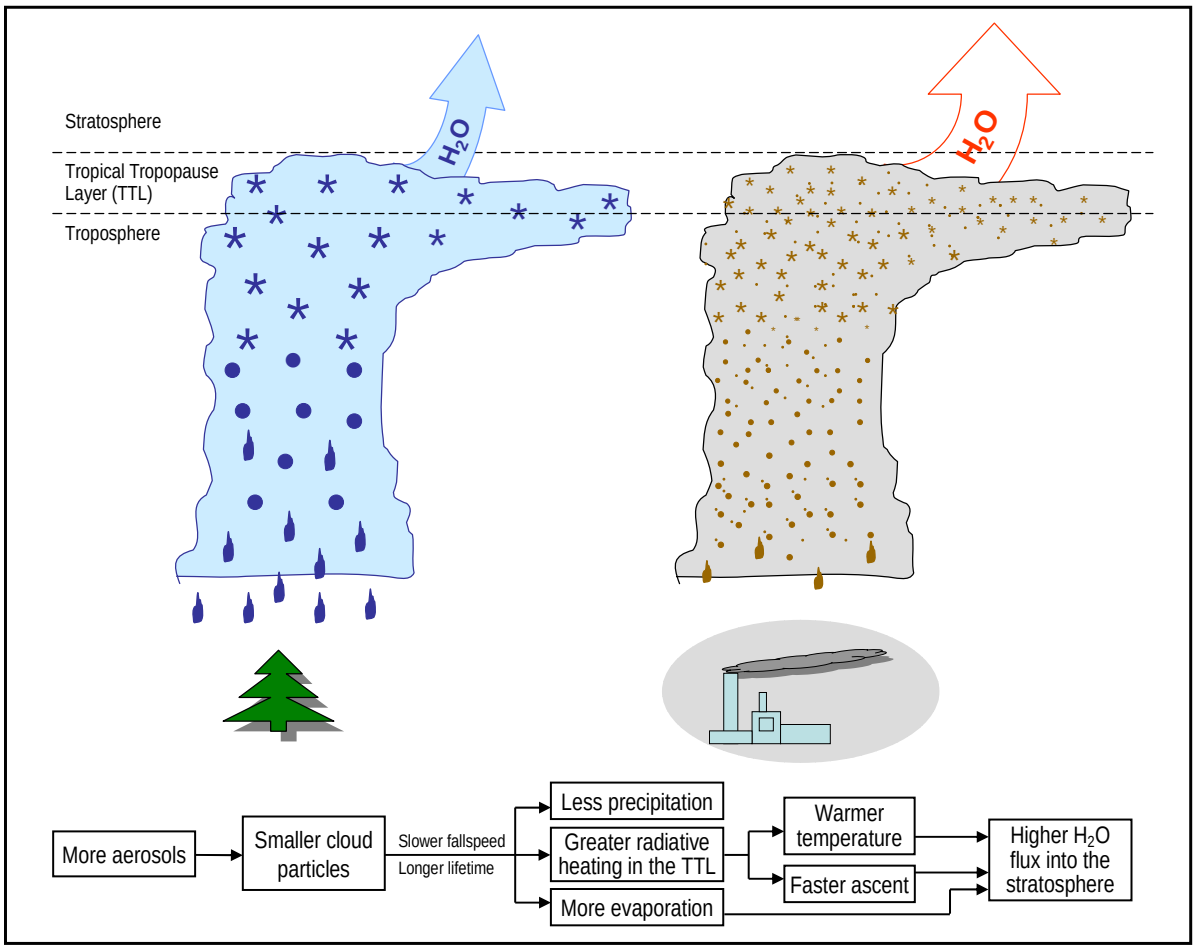
Stratosphere
Tropical Tropopause Layer (TTL)
Troposphere
H_2O
H_2O
More aerosols
Smaller cloud particles
Slower fallspeed
Longer lifetime
Less precipitation
Greater radiative heating in the TTL
More evaporation
Warmer temperature
Faster ascent
Higher H_2O flux into the stratosphere

Figure 5